RSC Advances

PAPER

View Article Online
View Journal | View Issue

Cite this: *RSC Adv.*, 2016, **6**, 88762

Ultra-fast microwave-assisted reverse microemulsion synthesis of Fe_3O_4@SiO_2 core–shell nanoparticles as a highly recyclable silver nanoparticle catalytic platform in the reduction of 4-nitroaniline†

C. Y. Lu,*[ab] T. Puig,[b] X. Obradors,[b] S. Ricart[b] and J. Ros[a]

Received 1st August 2016
Accepted 12th September 2016

DOI: 10.1039/c6ra19435d

www.rsc.org/advances

A novel microwave-assissted reverse microemulsion method was applied to prepare Fe_3O_4@SiO_2 core–shell nanoparticles rapidly for the first time. The morphology of the core–shell structure is controlled by tunning the reaction parameters. Nanoparticles with a very thin SiO_2 coating layer (2.5 nm) containing a single Fe_3O_4 nanoparticle (8–9 nm) are produced. These core–shell nanoparticles can be used as solid catalytic supports for Ag nanoparticles and applied in 4-nitroaniline reduction. Transmission electron microscopy showed that the core–shell nanoparticles were decoracted with Ag nanoparticles of 7 nm in diameter. The crystal structures of the Fe_3O_4 and Ag nanoparticles were confirmed by X-ray diffraction. These Ag/Fe_3O_4@SiO_2 nanocomposites showed high catalytic efficiency and recycling properties even after 20 times of repetation.

Introduction

Due to their unique magnetic properties and biocompatibility, iron oxide nanoparticles have been intensively studied for the past few decades for wide applications in biotechnology, data storage, magnetic fluids and catalysis.[1,2] Nobel metal nanomaterials, like Au, Pt and Ag, are promising catalysts for many reactions, for example Au nanoclusters can be used in the selective oxidation of styrene[3] and Pt-based heterogeneous nanomaterials are promising catalysts in direct methanol fuel cells.[4] Ag nanoparticles have also been comprehensively studied for their promising application in biotechnology and catalysis. Compared with other noble metal nanoparticles, such as Au, Pt and Pd, Ag nanoparticles are cheaper and have some special properties like antibacterial activity, plasmon resonant optical properties and an enhancing the effect of radiation treatment, which make them ideal candidates for biomarkers, optical sensors and antimicrobial drugs.[5,6] It is also worth noting that using Ag NPs as the catalyst to reduce nitroaniline would be an effective and environmentally friendly procedure to synthesize amino compounds.[7]

Because of the multifunctional requirement, Fe_3O_4/Ag composite materials with the combination of excellent magnetic properties, biocompatibilities and plasmonic properties would be a promising composite for multiple applications. However the uncovered Fe_3O_4 NPs were easy to oxidized and aggregated during the preparation and application process. The chemical and thermal stable silica layers could be a nice candidate for decorating and protect the iron oxide nanoparticles' surface. And the nontoxic silica provides Fe_3O_4 nanoparticles with water solubility as well as good biocompatibility, which has potential applications in bio-imaging and drug delivery.[8] For the research in functional materials, Fe_3O_4@SiO_2@Y_2O_3:Eu_3^+ core–shell structures have magnetic response performance and luminescent properties[9] and the Fe_3O_4@SiO_2@Au core–shell microspheres exhibit an enhancement ability of surface-enhanced Raman scattering for rhodamine-b detection.[10]

Nowadays, Stöber method[11–16] and reverse microemulsion system[17–24] were both widely used to prepare Fe_3O_4@SiO_2 core–shell structures. Fe_3O_4@SiO_2 core–shell nanoparticles with ultra-thin silica shell (~2 nm) and a high saturated magnetization (15 emu g^{-1})[25] can be synthesized through reverse microemulsion method.[26–28] However, both methods requires long time for SiO_2 condensing, taking around 24 h for one reaction.[29] This is a great disadvantage that hinders the fast and massive production of Fe_3O_4@SiO_2 core/shell nanoparticles and their wide application.

[a]*Departament de Quimica, Edifici C Facultat de Ciències, Universitat Autònoma de Barcelona (UAB), Cerdanyola del Vallès, Barcelona 08193, Spain. E-mail: lu.changyong@e-campus.uab.cat*

[b]*Institute of Materials Science of Barcelona (ICMAB-CSIC), Campus de la UAB, Cerdanyola del Vallès, Barcelona 08193, Spain*

† Electronic supplementary information (ESI) available: Electron diffraction pattern, thermal gravity cure, weight percentage calculation and elements mapping test. See DOI: 10.1039/c6ra19435d

Microwave irradiation significantly accelerates the reaction rate, increases yields and reduces side reactions in the preparation of different kinds of nanoparticles, from metals to oxides and semiconductors.[30–32] The synthesis of NPs@SiO_2 core–shell structure were only reported by using microwave assistance Stöber method,[33,34] and the fast preparation of core–shell nanoparticles with controllable small size and very thin SiO_2 layer remain challenging. The combination of microwave irradiation and reverse microemulsion method has the possibility to overcome this problem, to our knowledge, this method was used until now to prepare Au NPs, zincophosphates,[35] MOF[36] and zeolite nanocrystals[37] and the results indicate that this method has great improvement on yield, size distribution and reducing the reaction than the normal reverse microemulsion method.

In this work, we report a novel rapid approach based on microwave assisted reverse microemulsion process to synthesize Fe_3O_4@SiO_2 core–shell nanoparticles with a very thin SiO_2 layer (2.5 nm in average) within only 5 min (Fig. 1). The synthesized core–shell structures were stable in ethanol and well-formed. Moreover these Fe_3O_4@SiO_2 core–shell nanoparticles were further functionalized with (3-aminopropyl)triethoxysilane (APTES) and decorated with Ag nanoparticles. The morphology and crystal structure of Fe_3O_4@SiO_2 and Fe_3O_4@SiO_2/Ag nanoparticles were analysed through different techniques for example transmission electron microscopy (TEM), high resolution transmission electron microscopy (HR-TEM) and X-ray diffraction (XRD) and the magnetic properties were measured by superconducting quantum interference device (SQUID). The catalytic efficiency and recycling test were done *via* monitoring the 4-nitroaniline reduction reaction. The morphology of nanoparticles, such as the aggregation and the number of core particles, can be well manipulated through changing the amount of reactants. This kind of core–shell nanoparticle is superparamagnetic with a relatively high saturation magnetization value 32.7 emu g^{-1}.[27] This kind of core–shell nanoparticle could be used as the support for Ag nanoparticles and the synthesized Fe_3O_4@SiO_2/Ag nanocomposites show great catalytic and recycling properties.

Experimental details

Materials

Iron(III) acetylacetonate (99.9%), benzyl ether (98%), oleic acid (90%), oleylamine (70%), triethylene glycol (99%), cyclohexane (99%), Igepal CO-520 (average M_n 441), ammonium hydroxide solution (30–33% NH_3 in H_2O), tetraethyl orthosilicate (98%), (3-aminopropyl)triethoxysilane (APTES, 99%), sodium borohydride (98%), silver nitrate (99%) and 4-nitroaniline (99%) were used as received from Sigma-Aldrich (Madrid Spain). *n*-Hexane (96%) was used as received from Scharlab (Barcelona Spain). Ethanol (absolute PA 99.5%) was used as received from PanReac AppliChem (Barcelona Spain).

Synthesis of Fe_3O_4 nanoparticles

The oleic acid and oleylamine capped Fe_3O_4 nanoparticles were prepared through a modified way of the decomposition of iron oleate complex described somewhere else.[1] In a typical synthesis, 1 mmol iron(III) acetylacetonate was dissolved in 20 ml benzyl ether then 3 mmol oleic acid, 3 mmol oleylamine and 5 mmol triethylene glycol were subsequently added into the solution, followed by transfer the mixture to a two neck round bottom flask with magnetically stirred under N_2 flow for at least 30 min to eliminate the oxygen inside the vial. The mixture was heated to 200 °C at heating rate 1 °C min^{-1} and kept for 30 min. Then the mixture was heated to 265 °C under the same heating rate and hold for another 30 min. The black solution was cooled to room temperature naturally. All the experiments were under refluxing process and N_2 flow. The Fe_3O_4 nanoparticles were precipitated by adding ethanol, collected by centrifugation (10 000 rpm, 10 min) and dispersed in 20 ml hexane with 0.14 mmol oleic acid and 0.152 mmol oleylamine inside. Then the solution was centrifuged to 6000 rpm for 10 min to eliminate the insoluble part, excessive ethanol was subsequently added into the solution to precipitate the nanoparticles, the solids were collected through centrifugation at 10 000 rpm for 10 min and dispersed in 20 ml hexane and used in the preparation of Fe_3O_4@SiO_2 core–shell nanoparticles.

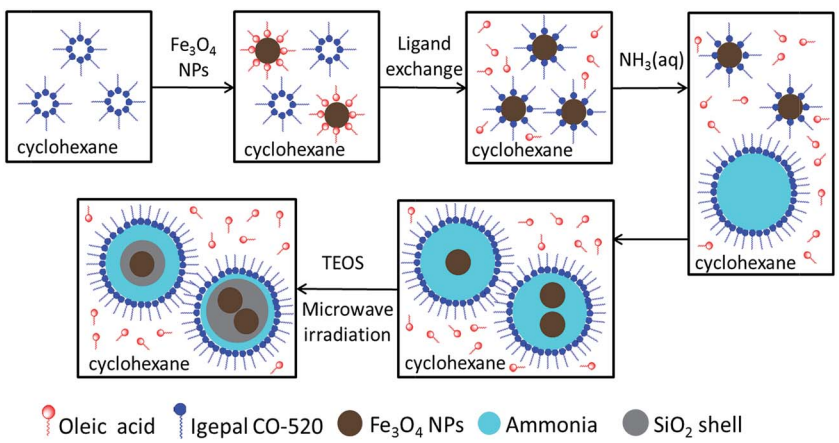

Fig. 1 Synthesis of Fe_3O_4@SiO_2 core–shell nanoparticles.

Synthesis of Fe_3O_4@SiO_2 core–shell nanoparticles

In this process, different volume of Igepal CO-520 (1 ml, 1.5 ml, 2 ml corresponding to 200 mM, 300 mM, 400 mM in concentrations) were dissolved in 10 ml cyclohexane and stirred for 30 min, then 0.36 ml of as prepared Fe_3O_4 nanoparticles solution was added into the solution and stirred for 3 h followed by adding a variety concentration of ammonium hydroxide solution (71 mM, 141 mM, 211 mM and 280 mM) into the solution and kept stirring for 1 h to form a transparent water in oil (w/o) micro emulsion system. Finally the solution was mixed with 10 μl of tetraethyl orthosilicate in a microwave reaction vessel. The program was set as follows, the solution was stirred for 2 min in the first step then quickly heated up to 60 °C with the maximum operation power of 300 W and hold for 5 min, then cooled down to room temperature. The solid was precipitated by adding ethanol and washed with ethanol through centrifugation (10 000 rpm 10 min) for several times and finally the Fe_3O_4@SiO_2 core–shell nanoparticles were dispersed in 10 ml ethanol.

Synthesis of Fe_3O_4@SiO_2/Ag nanocomposites

Before the decoration of Ag nanoparticles, the Fe_3O_4@SiO_2 core–shell nanoparticles were first functionalized with $-NH_2$ group. In a typical reaction 3 ml of synthesized core–shell nanoparticles suspension were diluted in 15 ml of distilled water with 0.1 ml of ammonia inside and ultrasound for 30 min, then 10 μl of (3-aminopropyl)triethoxysilane (APTES) was added into the solution follow by heating the mixture to 60 °C and keep stirring for 2 h. The nanoparticles were collected through centrifuge treatment (10 000 rpm, 30 min) and washed for several times with water and ethanol. Then disperse them in 20 ml water with ultrasound treatment for 30 min. After that, 0.5 ml of $AgNO_3$ aqueous solution (0.01 M) was added into the mixture with continues stirring in ice water bath, then 1 ml of $NaBH_4$ aqueous solution (0.01 M) was injected into the solution drop by drop to make a slowly formation of Ag nanoparticles. The mixture was stirred for another 2 h to get a black solution. Finally the Fe_3O_4@SiO_2/Ag nanocomposites were obtained through centrifuge (1000 rpm, 20 min) and washed several times with water and ethanol.

Catalytic test

To study the catalytic properties of our synthesized Fe_3O_4@SiO_2/Ag nanocomposites, we use them in the reduction of 4-nitroaniline to 4-phenylenediamine. In a typical reaction, 400 μl of 1 mM 4-nitroaniline aqueous solution, 400 μl of 10 mM $NaBH_4$ aqueous solution and 200 μl of Fe_3O_4@SiO_2/Ag aqueous suspension were dispersed in 1 ml of H_2O. The reduction reaction was monitored through a UV-visible spectrophotometer in a quartz cuvette with 10 mm path length and with freshly made solutions. To study the recycling properties of Fe_3O_4@SiO_2/Ag nanocomposites, the exactly same process was repeated for 20 cycles. The nanoparticles were separated from the solution by simply applying a external magnetic field and washed for 2 times with distilled water for the following reduction reaction.

Characterization methods

Fourier transform infrared spectroscopy (ATR-FT-IR) was performed on a Bruker Tensor[27] Fourier transform infrared spectrometer (Golden gate) in a range of 600–4000 cm^{-1}. All samples were measured in solid form at room temperature.

Transmission electron microscope (TEM) and high resolution transmission electron microscopy (HR-TEM) measurements were conducted on a JEOL 1210 TEM microscopy at 130 kv and a JEM-2011 HR-TEM microscopy at 200 kv. One drop of the hexane suspension of Fe_3O_4 nanoparticles and ethanol suspension of Fe_3O_4@SiO_2 and Fe_3O_4@SiO_2/Ag nanoparticles were deposited on the carbon-coated copper grids respectively. In order to minimize the aggregation of nanoparticles, the copper grids were laid on a filter paper during the drying process.

X-ray powder diffraction studies (XRD) were performed on D5000 Siemens X-ray powder diffractionmeter in a reflection mode by using Cu Kα $\lambda = 1.5406$ Å radiation in a range of $10^\circ \leq 2\theta \leq 80^\circ$.

The field-dependent magnetization curves were characterized by SQUID (Quantum design MPMS XL-7T) under a magnetic field from 0 to ±70 000 Oe at 5 K.

The thermogravimetric analysis (TGA) was carried on a NETZSCH-STA 449 F1 Jupiter thermal analysis system from room temperature to 800 °C under a O_2 flow.

Particle size distribution tests were implemented on a Zetasizer Nano Z system from Malvern Instruments (He–Ne laser 633 nm, Max 4 mW) by dynamic light scattering.

The catalytic reaction was characterized by a Varian Cary 5000 UV-Vis-NIR spectrophotometer operated at 1 nm resolution using freshly made solution in quartz cuvettes with 10 mm path length.

Results and discussion

Fig. 3a and S1 (ESI†) display the TEM images of Fe_3O_4 NPs prepared using a modified previous published method.[38] The XRD measurements (Fig. 2) of both types of nanoparticles agree with the standard Fe_3O_4 XRD pattern (JCPDS no. 16-629) showing clearly the characteristic (220), (311), (400), (422), (511) and (440) diffraction peaks which also identify with the electron diffraction of Fe_3O_4 nanoparticles (Fig. S2, ESI†). The XRD pattern of Fe_3O_4@SiO_2 nanoparticles shows a wide peak around 20–25° which is ascribed to the amorphous silica shell, besides of this peak, the rest of diffraction peaks all belong to the characteristic peaks of the cubic structure of Fe_3O_4 nanoparticles.

In the FT-IR curve of Fe_3O_4 nanoparticles (Fig. 3b red line), the absorption peaks at 2192 cm^{-1}, 2850 cm^{-1} are attributed to $-CH_2$ stretching vibration and 1708 cm^{-1} is coming from C=O stretching modes of dimeric COOH groups and the peaks at 1406 cm^{-1} could be ascribed to the coupling of hydroxyl bending vibration with C–O stretching vibration. The absorption band at 1598 cm^{-1} is the characteristic peak of C=C vibration and the peak at 1522 cm^{-1} is belonging to the COO^- asymmetric stretching vibration. All those peaks indicate that

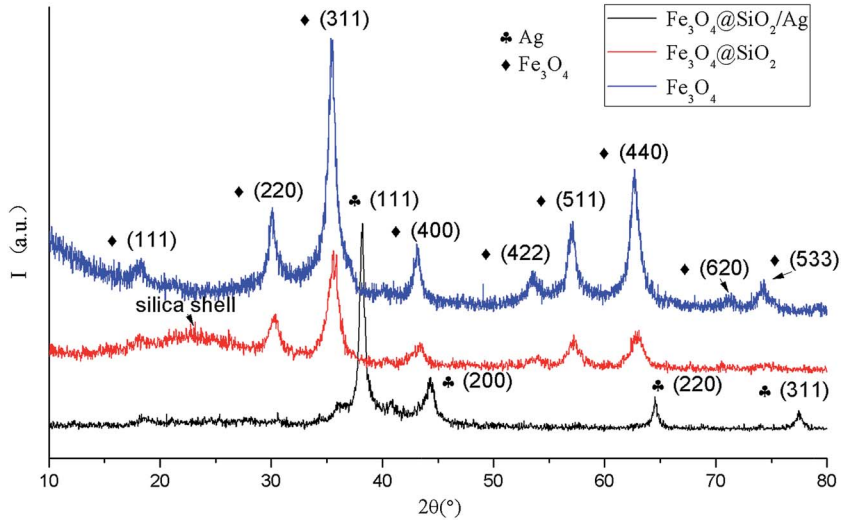

Fig. 2 XRD patterns of Fe_3O_4, Fe_3O_4@SiO_2 core–shell nanoparticles and Fe_3O_4@SiO_2/Ag nanocomposites.

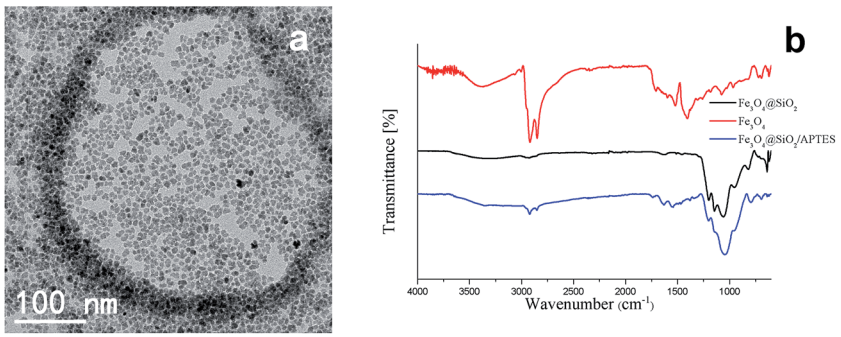

Fig. 3 TEM image of Fe_3O_4 NPs (a) and FT-IR curve of Fe_3O_4 nanoparticles, Fe_3O_4@SiO_2 core–shell nanoparticles and Fe_3O_4@SiO_2-APTES nanoparticles (b).

the oleic acid is absorbed on the Fe_3O_4 nanoparticles which results in a well dispersion of Fe_3O_4 in hexane. After the microwave irradiation, the FT-IR curve of Fe_3O_4@SiO_2 (Fig. 3b black line) shows two small peaks in 1512 cm^{-1}, 1457 cm^{-1} coming from stretching vibration of aromatic ring C=C and two strong peaks in 1200 cm^{-1} and 1060 cm^{-1} which attribute to the symmetric stretching vibration of =C–O–C and asymmetric stretching vibration of =C–O–C. The existence of those vibration models indicates that there are still some amounts of Igepal CO-520 attached on the nanoparticles' surface. The absorption bands at 1145 cm^{-1}, 953 cm^{-1}, 819 cm^{-1} attribute to the vibration models of SiO_2 which means that the SiO_2 were successfully covered on the Fe_3O_4 nanoparticles. The FT-IR results indicate the substitution of oleic acid and oleylamine capping ligands for the silica shell after microwave process. Strong bands centered at 820 cm^{-1} can be unequivocally attributed to the vibration modes of SiO_2.

TEM studies of Fe_3O_4@SiO_2 core–shell nanoparticles prepared with microwave assistance and normal reverse microemulsion methods (Fig. 4a and b) prove that the core–shell structure is obtained through both methods but the size of

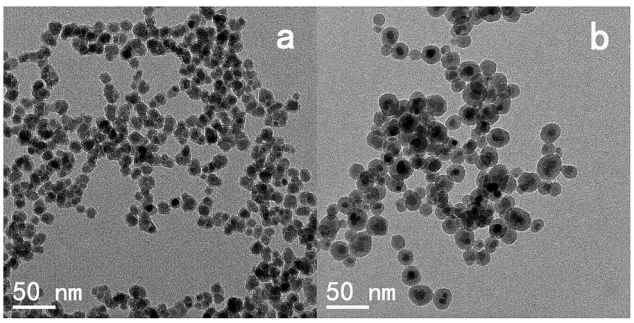

Fig. 4 TEM images of Fe_3O_4@SiO_2 core–shell nanoparticles prepared by microwave irradiation (a) and normal reverse microemulsion process (b).

samples are significantly different: the shell thickness is 6.6 nm and total size is about 30 nm for the normal reverse microemulsion method, on the other hand the shell is only 2.5 nm thick and total size is about 14 nm for the microwave assisted reaction. The thinner shell of microwave irradiation method could be ascribed to the short irradiation time during the TEOS

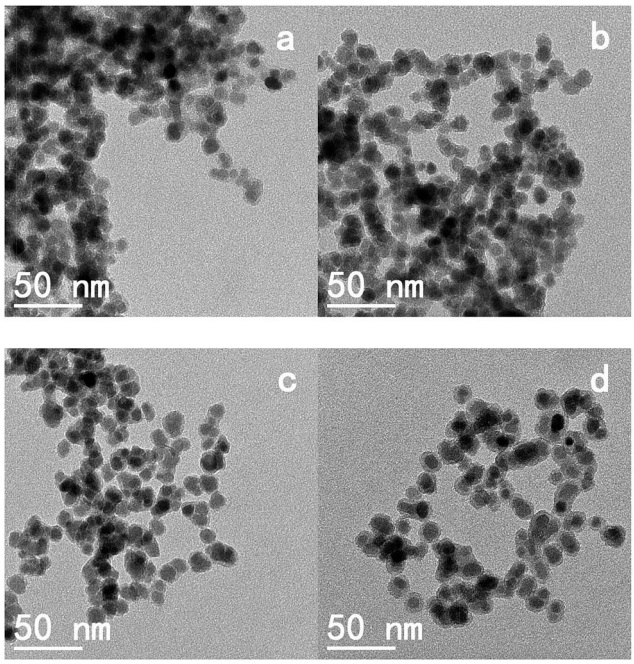

Fig. 5 TEM images of Fe_3O_4@SiO_2 nanoparticles synthesized by microwave assisted reverse microemulsion method with different concentration of ammonia inside, 71 mM (a), 141 mM (b), 211 mM (c) and 280 mM (d).

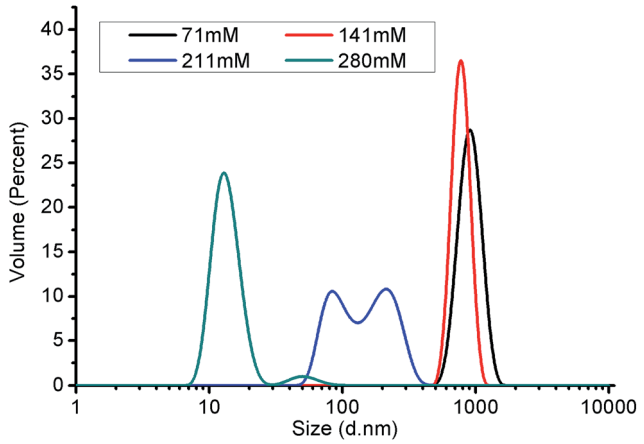

Fig. 6 Particle size distribution of Fe_3O_4@SiO_2 core–shell nanoparticles prepared under different concentration of ammonia.

Table 1 Shell thickness of Fe_3O_4@SiO_2 core–shell nanoparticles prepared with different concentration of ammonia

Concentration of ammonia	71 mM	141 mM	211 mM	280 mM
Shell thickness	2.51 nm	2.55 nm	2.54 nm	2.60 nm

hydrolysis reaction. It is worth to mention that the synthesized core–shell nanoparticles are not porous which made them unable combine the multifunctional capping agents with highly loading percentage compare to the recent reports about mesoporous silica nanocarriers.[39,40]

In order to optimize the silica shell formation, different concentrations of ammonia (71 mM, 141 mM, 211 mM and 280 mM) were used in each reaction. The TEM images (Fig. 5a–d) of core–shell nanoparticles show that after the microwave process a 2–3 nm thickness shell was formed. As is presented in Fig. 4 ammonia concentrations up to 211 mM give dispersions of particles with a chain like structure. Progressive increase of the amount of ammonia produced an improvement the dispersion reaching monodisperse core–shell NPs with ammonia concentration to 280 mM (Fig. 5d). DLS studies (Fig. 6) indicate that the samples prepared by using 71 mM and 141 mM ammonia show big aggregation and the sample synthesized by adding 211 mM ammonia shows a mixture of relative small size nanoparticles and big size aggregation. When 280 mM ammonia was used in the reaction, the DLS result (Fig. 6) shows that most of core–shell nanoparticles are about 15 nm which is in agreement with TEM results (Fig. 5). This effect can be explained by the role of ammonia in decorating the condensed SiO_2 surface that results in a more negatively charged layer, leading to a better dispersion of Fe_3O_4@SiO_2 nanoparticles. It should be pointed out that in this method the increasing concentration of ammonia does not affect the shell thickness of nanoparticles (see Table 1), whereas the shell thickness were changed with different concentration of ammonia in conventional reverse microemulsion method (see Table S1, ESI†). This effect might come from the short reaction time and ammonia evaporation during the microwave irradiation. The controll of shell thickness is under study.

The effect of the amount of surfactant was also studied. Increasing the amount of surfactant (Igepal CO-520) in the reaction produced a progressive decrease of the number of nanoparticles in the core (see Fig. 7a–c) and finally single-core core–shell nanoparticles were achieved using 400 mM surfactant. Based on the chemical mechanism previously discussed by Wang *et al.*,[20] the molar ratio of water and surfactant (Igepal CO-520 in our case) is very important for the morphology and particle size of core–shell structures. The increase of water/surfactant ratio produces the increase of micelles size facilitating intermicellar nucleation processes. For this reason, there were more nanoparticles inside the core of the sample than the other samples when 200 mM of Igepal CO-520 was employed at the first step of micelle formation.

Fe_3O_4@SiO_2 core–shell nanoparticles prepared by microwave irradiation display a strong magnetism that allows their

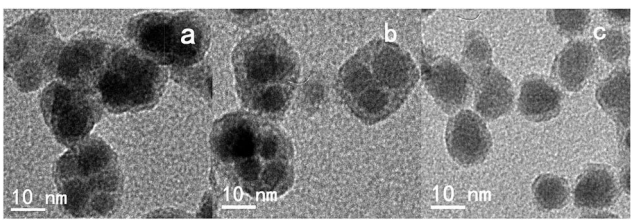

Fig. 7 TEM images of Fe_3O_4@SiO_2 core–shell nanoparticles prepared with different concentration of Igepal CO-520 inside, 200 mM (a), 300 mM (b) and 400 mM (c).

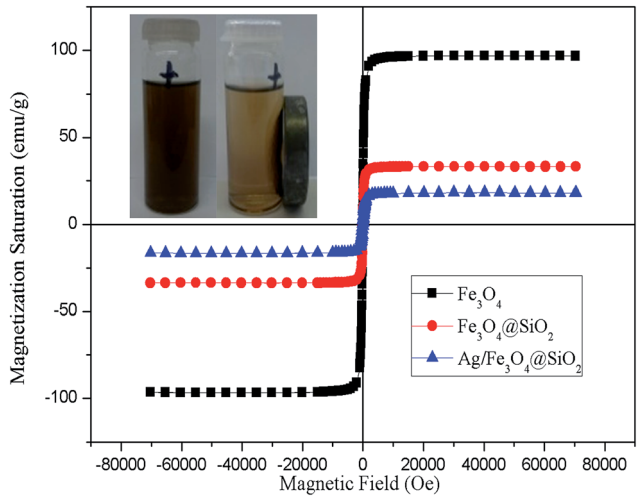

Fig. 8 Field-dependent magnetization curves (5 K) for the prepared Fe_3O_4, Fe_3O_4@SiO_2 core–shell and Ag/Fe_3O_4@SiO_2 nanoparticles measured by SQUID and a photo of Ag/Fe_3O_4@SiO_2 nanoparticles dispersed in water in the absence and presence of magnetic field (insert).

separation from the solution with a magnet. Fig. 8 shows the magnetization test of Fe_3O_4 and Fe_3O_4@SiO_2 core–shell nanoparticles. Magnetite nanoparticles are superparamagnetic with a high saturation magnetization value (96.9 emu g^{-1}). After covered by silica shell, the nanoparticles display a lower saturation magnetization (32.7 emu g^{-1}) but the core–shell structure remains superparamagnetic. Based on the calculation of weight percentage (ESI†) of Fe_3O_4 in the core–shell structure, the magnetization of Fe_3O_4 nanoparticles didn't change to nonmagnetic phase during the reaction. The magnetic properties of as prepared core–shell nanoparticles are comparable to other reported in the literature.[20]

The magnetic materials were widely used as the support for catalysis. For example, palladium catalysts were loaded on the Ni MOF-derived N-doped magnetic mesoporous carbon for the hydrodechlorination reaction of chlorophenols.[41] In this paper silver nanoparticles were synthesized on the surface of Fe_3O_4@SiO_2 core–shell nanoparticles. The obtained core–shell nanoparticles were first functionalized with $-NH_2$ group (see Fig. 3b blue line) by using APTES molecule. The weak absorption peaks between 1490 cm^{-1} and 1631 cm^{-1} and at 3352 cm^{-1} attribute the NH_2 group of APTES and the peaks at 2922 cm^{-1} and 2852 cm^{-1} coming from the propyl chain of APTES molecule, all these peaks indicate the successful functionalization of $-NH_2$ group on the surface of core–shell nanoparticles. The silver nanoparticles were formed and decorated on the surface of silica shell through a simple reduction reaction. The XRD pattern of Ag/Fe_3O_4@SiO_2 nanocomposites (Fig. 2) indicates that strong diffraction peaks which identify with the standard Ag diffraction pattern (JCPDS no.04-0783) showing the characteristic (111), (200), (220) and (311) peaks. Fig. 9 shows the TEM images of Ag/Fe_3O_4@SiO_2 nanoparticles. From the images, the well-dispersed sliver nanoparticles were found to attach to the surface of core–shell nanoparticles with an average diameter

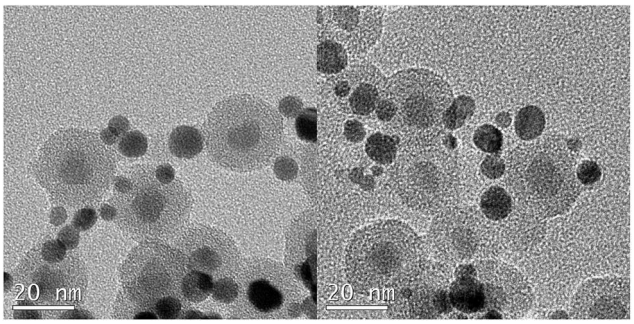

Fig. 9 TEM images of Ag/Fe_3O_4@SiO_2 nanoparticles.

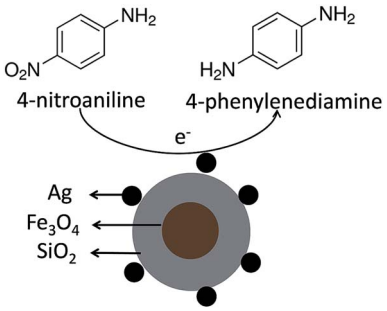

Fig. 10 Reaction mechanism about the reducing 4-nitroaniline when using Ag/Fe_3O_4@SiO_2 nanocomposites as the catalysts.

about 7 nm. It is noteworthy that the shell thickness of silica is thicker than the pictures in Fig. 7 which could be attributed to the process of functionalization the shell with APTES. The high angle annular dark-field scanning TEM (HAADF-STEM) image and corresponding elements mapping images (Fig. S5 ESI†), confirmed the Fe atoms were only distributed in the core and the Si atoms were homogeneously distributed around the Fe_3O_4 core, indicated a clearly core–shell structure. In the mean while the Ag atoms were main distributed outside the SiO_2 shell suggested a successfully decoration of Ag nanoparticles on the surface of Fe_3O_4@SiO_2 core–shell nanoparticles.

The decoration of silver nanoparticles on the Fe_3O_4@SiO_2 core–shell structure causes a further decrease in the magnetic saturation value to 18.2 emu g^{-1} (Fig. 8), which was attribute to the mass effect of silver and silica. The Ag/Fe_3O_4@SiO_2 nanocomposites showed a strong magnetization which makes it separated by external magnetic field (see Fig. 8 insert image), indicates that this nanocomposites are suitable for magnetic separation and targeting.

The principal of the reduction reaction of 4-nitroaniline to 4-phenylenediamine when using Ag/Fe_3O_4@SiO_2 nanocomposite as the catalysis is showed in Fig. 10. This reaction is considered quite useful in the synthesis of rubber and polymer product[42,43] and the catalytic reduction of nitro-compound is well studied.[44] The whole reduction reaction could be easily monitored by the UV-vis spectroscopy through the decrease if the strong absorption peaks at 380 nm which could be attribute to 4-nitroanilinate anion. In the Fig. 11, a dramatically decreased of absorption peak at 380 nm when using Ag/Fe_3O_4@SiO_2 as the

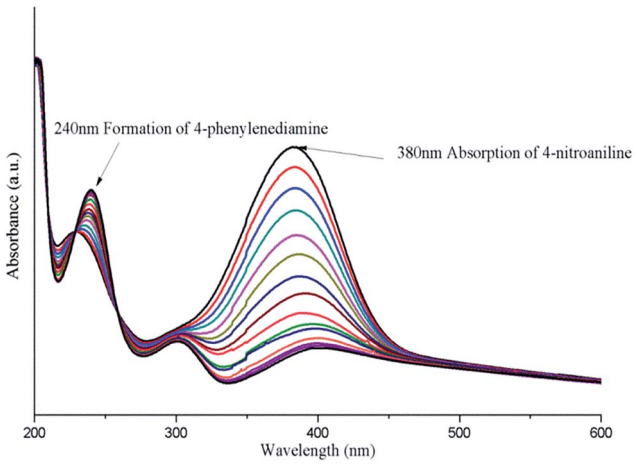

Fig. 11 UV-visible spectra for the reaction of 4-nitroaniline molecule by Ag/Fe_3O_4@SiO_2 nanocomposites at various times.

catalysis, meaning while a peak at 240 nm was appeared and getting stronger with the increase of reaction time which related to the 4-phenylenediamine. Based on the previous report, the reduction reaction happened through the transfer of electrons from the 4-nitroaniline molecules as long as both compounds attached on the surface of Ag/Fe_3O_4@SiO_2 nanocomposites. When the electron transferred to Ag nanoparticles the hydrogen atoms formed and attacked the 4-nitroaniline molecules leading to the occurrence of reduction reaction.[45] It is noteworthy that the 4-nitroaniline could be fully reduced within 5 min when using our synthesized Ag/Fe_3O_4@SiO_2 nanocomposites as the catalysis. This phenomenon could be explained by the high surface activity of Ag nanoparticles and the large surface area provided by the small size core–shell nanoparticles. These two characters ensure the Ag/Fe_3O_4@SiO_2 nanocomposites have a good catalytic property. And the TOF value was also calculated to 6 h^{-1}.

Another advantage of our synthesized Ag/Fe_3O_4@SiO_2 nanocomposite is high recyclability compared to the single Ag nanoparticles catalysts. The recycling test of Ag/Fe_3O_4@SiO_2 catalysis demonstrated that about 86% of 4-nitroaniline was reduced even after 20 cycles (see Fig. 12). It is worth to note that the nanoparticles start to aggregate after 20 cycles (Fig. S6†) and there were still many Ag nanoparticles located outside the aggregates. The unique core–shell structure makes the nanocomposites highly stable and easily separated by magnet results in a quite well reutilization property compared to other similar studies.[46]

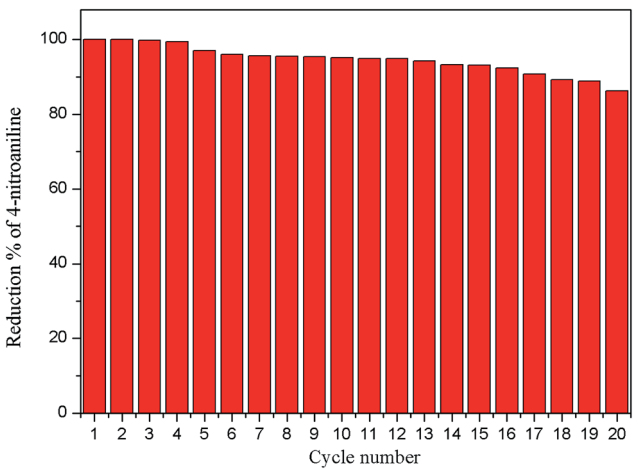

Fig. 12 The recycling curves of the catalyst Fe_3O_4@SiO_2/Ag for 20 repetitions.

Conclusions

A novel combination of reverse microemulsion system with microwave irradiation route was developed to prepare monodispersed Fe_3O_4@SiO_2 core–shell nanoparticles with a core–shell structure in a very short time. The magnetic nanoparticles were coated by a very thin layer of SiO_2 and the dispersity can be controlled by changing the volume of ammonia. On the other hand the number of nanoparticles inside the core could be tuneable through varying the concentration of surfactant (Igepal CO-520). Core–shell nanoparticles were superparamagnetic with a magnetization saturation value of *ca.* 32% of pure magnetite nanoparticles and the Fe_3O_4@SiO_2 nanoparticles were decorated by Ag nanoparticles. The produced Ag/Fe_3O_4@SiO_2 nanocomposites show nice catalytic efficiency and recycling property up 83% reduction of 4-nitroaniline after 20 cycles. This kind of core–shell structure materials can be also used in biomedical detection, drug delivery and battery system. It is also reasonable to believe that this new stagey is promising in rapid and massive production of various core–shell structure nanoparticles due to its time saving, facile and reliable properties.

Acknowledgements

This work was supported by an EU project (Eurotapes, FP7/2007-2013 NMP3-LA2012-280432) and Generalitat de Catalunya (Pla de Recerca 2009-SGR-770 and XaRMAE). We acknowledge the Universitat Autònoma de Barcelona and Institute of Materials Science of Barcelona (ICMAB) in particular Bernat Bozzo and Dr Judith Oro for helping in the characterization of the materials. A pre-doctoral fellowship from the China Scholarship Council is also acknowledged.

Notes and references

1 S. Laurent, D. Forge, M. Port, A. Roch, C. Robic, L. V. Elst and R. N. Muller, *Chem. Rev.*, 2008, **108**, 2064.
2 J. M. Jeong, B. G. Choi, S. C. Lee, K. G. Lee, S. J. Chang, Y. K. Han, Y. B. Lee, H. U. Lee, S. Kwon, G. Lee, C. S. Lee and Y. S. Hun, *Adv. Mater.*, 2013, **25**, 6250.
3 J. Fang, B. Zhang, Q. Yao, Y. Yang, J. Xie and N. Yan, *Coord. Chem. Rev.*, 2016, **322**, 1.
4 J. Qu, F. Ye, D. Chen, Y. Feng, Q. Yao, H. Liu, J. Xie and J. Yang, *Adv. Colloid Interface Sci.*, 2016, **230**, 29.
5 L. Liu, F. Ni, J. Zhang, X. Jiang, X. Lu, Z. Guo and R. Xu, *Acta Biochim. Biophys. Sin.*, 2011, **43**, 316.

6 L. Wang, J. Luo, S. Shan, E. Crew, J. Yin and C. O. Zhang, *Anal. Chem.*, 2011, **83**, 8688.
7 P. Zhang, C. Shao, Z. Zhang, M. Zhang, J. Mu, Z. Guo and Y. Liu, *Nanoscale*, 2011, **3**, 3357.
8 G. C. Rajib and P. Santanu, *Chem. Rev.*, 2011, **112**, 2373.
9 L. Z. Tong, J. H. Shi, D. M. Liu, Q. H. Li, X. Z. Ren and H. Yang, *J. Phys. Chem. C*, 2012, **116**, 7153.
10 J. H. Shen, Y. H. Zhu, X. L. Yang, J. Zong and C. Z. Li, *Langmuir*, 2012, **29**, 690.
11 V. M. Masalov, N. S. Sukhinina, E. A. Kudrenko and G. A. Emelchenko, *Nanotechnology*, 2011, **22**, 275718.
12 H. Mohammad-Beigi, S. Yaghmaei, R. Roostaazad, H. Bardania and A. Arpanaei, *Phys. E*, 2011, **44**, 618.
13 B. Q. Lu, Y. J. Zhu, G. F. Cheng and Y. J. Ruan, *Mater. Lett.*, 2013, **104**, 53.
14 J. Zou, Y. G. Peng and Y. Y. Tang, *RSC Adv.*, 2014, **4**, 9693.
15 X. M. Ni, Z. Zheng, X. K. Xiao, L. Huang and L. He, *Mater. Chem. Phys.*, 2010, **120**, 206.
16 W. Stöber, A. Fink and E. Bohn, *J. Colloid Interface Sci.*, 1968, **26**, 62.
17 T. Tago, T. Hatsuta, K. Miyajima, M. Kishida, S. Tashiro and K. Wakabayashi, *J. Am. Ceram. Soc.*, 2002, **85**, 2188.
18 J. Lee, Y. Lee, J. K. Youn, H. B. Na, T. K. Yu, H. Kim, S. M. Lee, Y. M. Koo, J. H. Kwak and H. G. Park, *Small*, 2008, **4**, 143.
19 C. Vogt, M. S. Toprak, M. Muhammed, S. Laurent, J. L. Bridot and R. N. Müller, *J. Nanopart. Res.*, 2010, **12**, 1137.
20 J. Wang, Z. H. Shah, S. Zhang and R. Lu, *Nanoscale*, 2014, **6**, 4418.
21 F. Jiang, Y. Fu, Y. Zhu, Z. K. Tang and P. Sheng, *J. Alloys Compd.*, 2012, **543**, 43.
22 S. Santra, R. Tapec, N. Theodoropoulou, J. Dobson, A. Hebard and W. Tan, *Langmuir*, 2001, **17**, 2900.
23 X. Gao, K. M. K. Yu, K. Y. Tam and S. Chi Tsang, *Chem. Commun.*, 2003, **24**, 2998–2999.
24 A. Guerrero-Martínez, J. Pérez-Juste and L. M. Liz-Marzán, *Adv. Mater.*, 2010, **22**, 1182.
25 M. Zhang, B. L. Cushing and C. J. O'Connor, *Nanotechnology*, 2008, **19**, 085601.
26 Y. Zhu, F. Y. Jiang, K. Chen, F. Kang and Z. K. Tang, *J. Sol–Gel Sci. Technol.*, 2013, **66**, 180.
27 H. L. Ding, Y. X. Zhang, S. Wang, J. M. Xu, S. C. Xu and G. H. Li, *Chem. Mater.*, 2012, **24**, 4572.
28 M. T. C. Fernandes, R. B. R. Garcia, C. A. P. Leite and E. Y. Kawachi, *Colloids Surf., A*, 2013, **422**, 136.
29 F. Chen, W. Bu, Y. Chen, Y. Fan, Q. He, M. Zhu, X. Liu, L. Zhou, S. Zhang and W. Peng, *Chem.–Asian J.*, 2009, **4**, 1809.
30 C. O. Kappe, *Angew. Chem., Int. Ed.*, 2004, **43**, 6250.
31 D. Dallinger and C. O. Kappe, *Chem. Rev.*, 2007, **107**, 2563.
32 Y. J. Zhu and F. Chen, *Chem. Rev.*, 2014, **114**, 6462.
33 C. Stutz, I. Bilecka, A. F. Thunemann, M. Niederberger and H. G. Borner, *Chem. Commun.*, 2012, **48**, 7176.
34 J. C. Park, D. A. Gilbert, K. Liub and A. Y. Louie, *J. Mater. Chem.*, 2012, **22**, 8449.
35 J. W. Doolittle Jr and P. K. Dutta, *Langmuir*, 2006, **22**, 4825.
36 K. L. M. Taylor, W. J. Rieter and W. Lin, *J. Am. Chem. Soc.*, 2008, **130**, 14358.
37 Z. Chen, S. Li and Y. Yan, *Chem. Mater.*, 2005, **17**, 2262.
38 S. H. Sun, H. Zeng, D. B. Robinson, S. Raoux, P. M. Rice, S. X. Wang and G. X. Li, *J. Am. Chem. Soc.*, 2004, **126**, 273.
39 T. Zhao, N. Goswami, J. Li, Q. Yao, Y. Zhang, J. Wang, D. Zhao and J. Xie, *Small*, 2016, DOI: 10.1002/smll.201601420.
40 S. Yang, D. Chen, N. Li, Q. Xu, H. Li, F. Gu, J. Xie and J. Lu, *Small*, 2016, **12**, 360.
41 X. Cui, W. Zuo, M. Tian, Z. Dong and J. Ma, *J. Mol. Catal. A: Chem.*, 2016, **423**, 386.
42 L. H. Shu and L. Y. Wen, *Ann. Occup. Hyg.*, 2009, **53**, 289.
43 I. Yoshiaki and K. Massaaki, *J. Health Sci.*, 2000, **46**, 467.
44 M. Tian, X. Cui, C. Dong and Z. Dong, *Appl. Surf. Sci.*, 2016, **390**, 100.
45 B. Naik, S. Hazra, V. S. Prasad and N. N. Chosh, *Catal. Commun.*, 2011, **12**, 1104.
46 H. Woo, K. Lee, S. Park and K. H. Park, *Molecules*, 2014, **19**, 699.